Disorder and order in sheared colloidal suspensions

B. Morin and D. Ronis

Department of Chemistry, McGill University, 801 Sherbrooke Ouest, Montréal, Québec, Canada H3A 2K6

(Received 26 January 1996)

We study colloidal suspensions in a linearly sheared solvent using standard stochastic field equations, namely, a modified Navier-Stokes equation for the solvent's velocity, coupled with the continuity equation for the suspensions' number density. Unlike earlier approaches, active mixing is included, leading to distortions in the structure factor for wave vectors perpendicular to the flow direction. Depending on the nature of the colloidal interactions, the density of the suspension, and the magnitude of the shear, spatial correlations can be either enhanced or reduced. Moreover, in strongly interacting systems, a spinodal line can be found, above which the system is unstable to the formation of layers perpendicular to the shear gradient. We discuss how our theory may be used to understand shear thinning or shear thickening, and the transition to lamellar phases seen in simulations. [S1063-651X(96)03207-2]

PACS number(s): 82.70.−y, 64.60.My

I. INTRODUCTION

Colloidal dispersions contain charged or neutral particles that are suspended in a solvent which may also contain excess counterions. Typically, the energy of interaction between the colloidal particles is of the same order of magnitude as ions in a metal, while their size is of the order of a micrometer [1]. Hence the interaction energy density is tremendously reduced in comparison to the usual molecular systems, and consequently, colloidal systems are very soft. Colloidal suspensions exhibit gaseous, liquid, crystalline, and glassy phases [2–5], and this makes them attractive model systems for a wide range of studies, phase transitions and shear-induced melting being two standard examples. Since the size and/or average separation of the particles is on the same scale as the wavelength of light, their structure may be probed either using light scattering at low concentrations, or small-angle neutron scattering (SANS) at larger packing fractions.

Because of their unusual softness, the nonequilibrium behavior of colloidal suspensions is of particular interest. Following the experimental work of Clark and Ackerson [6], sheared colloidal suspensions have been widely studied [2,7–11]. Most studies of nonequilibrium phenomena focus on the response of either crystalline-phase or liquid-phase colloidal suspensions to an applied shear stress. In the former case, the primary interest lies with the shear melting transition, where a solid colloidal suspension is sheared until it becomes disordered and liquidlike. In some simulations [12], a reentrant solid phase is found as the shear rate is increased past the melting transition, and furthermore, in stronger solids (obtained by increasing the packing fraction and/or reducing the counterion concentration) a solid-solid transition was observed with no melting occurring. Finally, we note that while discontinuities in viscometric functions have been observed, reentrant crystallization has not been observed in real systems. Instead, long-wavelength patterns (e.g., stripes) can form [13] and these have been explained using a continuum viscoelastic hydrodynamic model in Ref. [14].

The second case involves shearing a system in the liquid state; this leads to a wide variety of behaviors in terms of the structure factor or the suspension's viscosity as a function of the shear rate [15] (and references therein). The effective viscosity of the suspension can exhibit three possible behaviors, namely, the viscosity may be independent of the shear, or it may increase or decrease as the applied shear strength increases. Respectively, these correspond to Newtonian behavior, to shear thinning, and to shear thickening. Shear thinning seems to be the initial reaction of most systems under shear, and can be explained in terms of the loss of order seen in the structure factor, cf. Ref. [16]. As the shear rate is increased further, shear thickening may or may not be seen depending on the physical parameters of the sheared system and on the maximum attainable shear rate. Reference [12] also suggests that for suspensions which are in a solid state at equilibrium, once shear melting has occurred, one recovers the same types of behaviors found in an initially liquid suspension.

In this paper we use a statistical field theory model to study the effect of a linear shear gradient on hard-sphere colloidal dispersions at different concentrations. We focus on the structure factor for wave numbers in the shear gradient direction since, as will be seen later, this is probably the key aspect in understanding the rich phenomena mentioned above. This work was motivated by experiments and numerical simulations ([17,18], and others) in which distortions of the structure factor are seen in the plane perpendicular to the flow direction of the solvent, and more specifically, in the direction of the shear gradient. No theory of colloidal suspensions in a solvent predicts such an effect, though an approach ignoring the solvent and based on the Smoluchowski equation [11] (with boundary conditions defined on the suspended particles' closest approach surface), led to an effect in the plane perpendicular to the shear flow direction. Their results, however, are drastically different from those presented here and the conclusion which may be drawn from their study relative to the behavior of the system under shear is actually opposite to ours.

In the next section, the model is presented both in the form of Langevin equations and in the Martin-Siggia-Rose (MSR) formalism [19], and the two-point correlation function is given to one-loop order. The calculation is done for a

general equilibrium structure factor $S^{(eq)}$ and the general form of the results is given. The high- and low-shear domains are clearly identified in terms of the self-diffusion of the colloid particles and the characteristic length of the equilibrium structure factor, and may thus be easily compared with experiment. Simple expressions for the small-shear limit as well as for the asymptotic high-shear behavior are found. In Sec. III calculations are performed for a system of hard spheres in the Percus-Yevick approximation. We conclude in Sec. IV, and details of calculations are given in the Appendix.

II. THEORY

The model presented in this section involves a stochastic field theory description, of an *a priori* coarse grained system, and is an extension of Ronis's linear fluctuating diffusion equation [7]. The number density $N(\mathbf{x},t)$, which is a continuous variable, represents the number of particles per unit volume, where naively, the unit volume should be large with respect to the interparticle separations. However, the success of these types of theories in describing nonequilibrium structural changes in solids (see, e.g., Ref. [20]) has shown that often, the above coarse graining requirements are too stringent, and that the so-called phase field models may be extended down to lengths of the order of the interface width, that is, to the order of the interatomic spacing. Consequently, the standard assumptions will be made that the fields are smoothly varying functions of time and space and are everywhere well behaved, implying of course that any boundary effects are neglected. The other field relevant to our problem is the local velocity of the fluid, $\mathbf{v}(\mathbf{x},t)$.

The equations of motion governing the evolution of these fields are

$$\frac{\partial N(\mathbf{x},t)}{\partial t} = D_0 \nabla^2 \mu(\mathbf{x},t) - \mathbf{v}(\mathbf{x},t) \cdot \nabla N(\mathbf{x},t) + \zeta(\mathbf{x},t), \quad (1)$$

$$\frac{\partial \mathbf{v}(\mathbf{x},t)}{\partial t} = \nu \nabla^2 \mathbf{v}(\mathbf{x},t) - \mathbf{v}(\mathbf{x},t) \cdot \nabla \mathbf{v}(\mathbf{x},t) - \frac{\nabla p(\mathbf{x},t)}{\rho}$$

$$+ \frac{k_B T}{\rho n_c} \nabla N(\mathbf{x},t) \mu(\mathbf{x},t) + \mathbf{f}(\mathbf{x},t), \quad (2)$$

where $\mu(\mathbf{x},t) = \int [d\mathbf{k}/(2\pi)^d] e^{-i\mathbf{k} \cdot \mathbf{x}} N(\mathbf{k},t)/S^{(eq)}(\mathbf{k})$, and with the Gaussian noise, whose moments are

$$\langle \zeta(\mathbf{x},t) \rangle = 0,$$

$$\langle \zeta(\mathbf{x},t) \zeta(\mathbf{x}',t') \rangle = 2 D_0 n_c (-\nabla^2) \delta(\mathbf{x}-\mathbf{x}') \delta(t-t'), \quad (3)$$

$$\langle \mathbf{f}(\mathbf{x},t) \rangle = \mathbf{0},$$

and

$$\langle f_i(\mathbf{x},t) f_j(\mathbf{x}',t') \rangle = 2 k_B T (\nu/\rho) [-\nabla^2 \delta_{ij} - \nabla_i \nabla_j (\tfrac{1}{3} + \gamma)]$$

$$\times \delta(\mathbf{x}-\mathbf{x}') \delta(t-t'), \quad (4)$$

and where n_c is the number density of colloid particles, ρ is the fluid density, D_0 is the diffusion constant of the suspensions in the solvent, ν is the kinematic viscosity, p is the local pressure, and γ is the ratio of the bulk viscosity to the shear viscosity. The definition of $\mu(\mathbf{x},t)$ follows from de Gennes's expression for a generalized diffusion operator

[21], as in Ref. [7]. The above equations are simply the continuity equation [Eq. (1)], which ensures conservation of the total number of colloidal particles, and the Navier-Stokes equation as modified by the inclusion of active mixing [Eq. (2)], which describes the kinetics of a viscous fluid, here the solvent. In addition, the solvent is assumed to be incompressible and the colloidal particles neutrally buoyant; hence $\rho =$ const, which implies, using the continuity equation, a divergenceless velocity field, and thus Eqs. (1) and (2) are complemented by the following relations:

$$\rho = \text{const}, \quad \nabla \cdot \mathbf{v}(\mathbf{x},t) = 0. \quad (5)$$

This transversality condition implies longitudinal terms such as the pressure gradient term in Eq. (2) and the term in $\nabla_i \nabla_j$ in the velocity noise correlation Eq. (4), which includes the bulk viscosity drop out. The relaxation of this condition implies the existence of sound waves, a situation which was studied in simple liquids by Machta *et al.* [22], who looked at the deformation of the Brillouin peaks caused by shear.

This system of equations has been used previously to study systems near a phase transition such as pure fluids near the liquid-gas transition and binary mixtures near the critical concentration [23–26]. Since we are not studying a phase transition but rather nonequilibrium effects within a liquid phase, some phenomenological differences arise. First, the entire equilibrium structure factor is used as opposed to that obtained from a square-gradient expansion of the free energy in the relevant order parameter near the transition. Furthermore, the assumption about the equilibrium particle distribution, translating into the simple relation between $\hat{D}(\mathbf{k})$ and the equilibrium structure factor specified above, due to de Gennes [21], was later shown to be a good approximation for colloidal suspensions [4]. Thirdly, the convective term is usually neglected since by naive power counting, it has an upper critical dimension of 2, and is thus irrelevant for $d>2$. In the case at hand, however, these arguments do not apply since we are not in the critical region [in fact, one might wonder how the convective term can disappear in any dimension since it ensures Galilean invariance of the equation; a proper renormalization group (RG) treatment using, for example, the Callan-Symanzik equation to obtain the scaling functions, shows that *a priori*, the coefficient of the convective term is not affected by a scale transformation, and thus remains present when $d>2$]. Nevertheless, it will be seen later that for realistic shear strengths, the convective term appearing in the Navier-Stokes equation is negligible.

Note that the Navier-Stokes equation for an incompressible fluid when no external forces are involved relaxes to a simple Gaussian equilibrium distribution. This essentially follows from the particular structure of the reversible term (the convective term), leaving a simple linear term as the irreversible part of the thermodynamic force, from which a fluctuation-dissipation theorem follows [27,28]. In the same way, the additional term involving the number density $N(\mathbf{x},t)$, which appears in Eq. (2) (sometimes referred to as the active-mixing term), enforces detailed balance and hence, in the absence of external perturbations, allows the system to reach thermodynamic equilibrium. Note that the active-mixing term is responsible for hydrodynamic interactions; i.e., fluctuations in N at one point in the system lead to fluctuations in the velocity, which in turn affect density fluctua-

tions at other points. In the limit of vanishing Prandtl number, the active-mixing couplings all involve the usual Oseen tensor. Finally, note that our theory does not explicitly include the effects associated with the hydrodynamic boundary conditions at the colloidal particles' surfaces, except through the form of the diffusion constant.

The stochastic equations (1) and (2) together with the

constraint, Eq. (5), may be cast in functional form from which the generating functional of cumulants and of vertex functions may be defined. This representation of fluctuating field equations, known as the MSR formalism [19], has the practical purpose of defining vertex functions which can be calculated in perturbation theory using Feynman diagrams. We first define the functional:

$$
\begin{aligned}
H[N,\widetilde{N},\mathbf{v},\widetilde{\mathbf{v}}]=\int \frac{d\mathbf{k}\,d\omega}{(2\pi)^{d+1}}\bigg[& k_B T(\nu/\rho)k^2\widetilde{\mathbf{v}}(\mathbf{k},\omega)\cdot\overset{\leftrightarrow}{\boldsymbol{\Phi}}_{\mathbf{k}}\cdot\widetilde{\mathbf{v}}(-\mathbf{k},-\omega)-(-i\omega+\nu k^2)\widetilde{\mathbf{v}}(\mathbf{k},\omega)\cdot\mathbf{v}(-\mathbf{k},-\omega) \\
& -\frac{i}{2}\int \frac{d\mathbf{k}'d\omega'}{(2\pi)^{d+1}}\widetilde{v}^{\alpha}(-\mathbf{k},-\omega)\mathbf{V}_{\mathbf{k}}^{\alpha;\beta\gamma}v^{\beta}(\mathbf{k}',\omega')v^{\gamma}(\mathbf{k}-\mathbf{k}',\omega-\omega') \\
& +\frac{i}{2}\int \frac{d\mathbf{k}'d\omega'}{(2\pi)^{d+1}}\widetilde{\mathbf{v}}^{\alpha}(-\mathbf{k},-\omega)U^{\alpha}(\mathbf{k},\mathbf{k}')N(\mathbf{k}',\omega')N(\mathbf{k}-\mathbf{k}',\omega-\omega')+D_0 n_c k^2\widetilde{N}(\mathbf{k},\omega)\widetilde{N}(-\mathbf{k},-\omega) \\
& -\widetilde{N}(\mathbf{k},\omega)\bigg(-i\omega+\frac{D_0 k^2}{S^{(\mathrm{eq})}(k)}\bigg)N(-\mathbf{k},-\omega)-i\int \frac{d\mathbf{k}'d\omega'}{(2\pi)^{d+1}}\widetilde{N}(\mathbf{k},\omega)k^{\alpha}v^{\alpha}(\mathbf{k}',\omega')N(\mathbf{k}-\mathbf{k}',\omega-\omega')\bigg],\quad (6)
\end{aligned}
$$

where $(\overset{\leftrightarrow}{\boldsymbol{\Phi}}_{\mathbf{k}})^{\alpha\beta}\equiv\delta^{\alpha\beta}-k^{\alpha}k^{\beta}/k^2$, $\mathbf{V}_{\mathbf{k}}^{\alpha;\beta\gamma}\equiv k^{\beta}(\overset{\leftrightarrow}{\boldsymbol{\Phi}}_{\mathbf{k}})^{\alpha\gamma}+k^{\gamma}(\overset{\leftrightarrow}{\boldsymbol{\Phi}}_{\mathbf{k}})^{\alpha\beta}$, $U^{\alpha}(\mathbf{k},\mathbf{k}')\equiv k_B T/(\rho n_c)(\overset{\leftrightarrow}{\boldsymbol{\Phi}}_{\mathbf{k}})^{\alpha\beta}k'^{\beta}[1/S^{(\mathrm{eq})}(\mathbf{k}-\mathbf{k}')-1/S^{(\mathrm{eq})}(\mathbf{k}')]$, $\delta^{\alpha\beta}$ is the Kronecker delta, the Greek superscripts denote Cartesian coordinates, and a sum over repeated indices is henceforth implied. The above functional may be used to construct the partition function as

$$
\begin{aligned}
Z[h,\widetilde{h},\mathbf{j},\widetilde{\mathbf{j}}]=\int \{\mathcal{D}N\}\{\mathcal{D}i\widetilde{N}\}\{\mathcal{D}\mathbf{v}\}\{\mathcal{D}i\widetilde{\mathbf{v}}\}\exp(-H[N,\widetilde{N},\mathbf{v},\widetilde{\mathbf{v}}])\exp\bigg[& \int \frac{d\mathbf{k}\,d\omega}{(2\pi)^{d+1}}[h(\mathbf{k},\omega)N(-\mathbf{k},-\omega) \\
& +\widetilde{h}(\mathbf{k},\omega)\widetilde{N}(-\mathbf{k},-\omega)]\bigg]\exp\bigg[\int \frac{d\mathbf{k}\,d\omega}{(2\pi)^{d+1}}[\mathbf{j}(\mathbf{k},\omega)\cdot\mathbf{v}(-\mathbf{k},-\omega)+\widetilde{\mathbf{j}}(\mathbf{k},\omega)\cdot\widetilde{\mathbf{v}}(-\mathbf{k},-\omega)]\bigg].\quad (7)
\end{aligned}
$$

Using the partition function, we can define the free energy functional in the usual way: $F[h,\widetilde{h},\mathbf{j},\widetilde{\mathbf{j}}]=-\ln Z[h,\widetilde{h},\mathbf{j},\widetilde{\mathbf{j}}]$. The latter functional generates all connected graphs, or cumulants. Finally, through a Legendre transformation, we obtain the vertex functional:

$$
\begin{aligned}
\Gamma[\langle N\rangle,\langle\widetilde{N}\rangle,\langle\mathbf{j}\rangle,\langle\widetilde{\mathbf{j}}\rangle]=F[h,\widetilde{h},\mathbf{j},\widetilde{\mathbf{j}}]+ & \int \frac{d\mathbf{k}\,d\omega}{(2\pi)^{d+1}}[h(\mathbf{k},\omega)\langle N(-\mathbf{k},-\omega)\rangle+\widetilde{h}(\mathbf{k},\omega)\langle\widetilde{N}(-\mathbf{k},-\omega)\rangle] \\
& +\int \frac{d\mathbf{k}\,d\omega}{(2\pi)^{d+1}}[\mathbf{j}(\mathbf{k},\omega)\cdot\langle\mathbf{v}(-\mathbf{k},-\omega)\rangle+\widetilde{\mathbf{j}}(\mathbf{k},\omega)\cdot\langle\widetilde{\mathbf{v}}(-\mathbf{k},-\omega)\rangle],\quad (8)
\end{aligned}
$$

with

$$
\langle N(\mathbf{k},\omega)\rangle=\frac{-\delta F[h,\widetilde{h},\mathbf{j},\widetilde{\mathbf{j}}]}{\delta h(-\mathbf{k},-\omega)}\bigg|_{h=\widetilde{h}=0;\mathbf{j},\widetilde{\mathbf{j}}=\mathbf{0}},
$$

$$
\langle\widetilde{N}(\mathbf{k},\omega)\rangle=\frac{-\delta F[h,\widetilde{h},\mathbf{j},\widetilde{\mathbf{j}}]}{\delta\widetilde{h}(-\mathbf{k},-\omega)}\bigg|_{h=\widetilde{h}=0;\mathbf{j},\widetilde{\mathbf{j}}=\mathbf{0}},\quad (9)
$$

and,
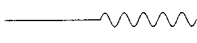
$$
\langle\mathbf{v}(\mathbf{k},\omega)\rangle=\frac{-\delta F[h,\widetilde{h},\mathbf{j},\widetilde{\mathbf{j}}]}{\delta\mathbf{j}(-\mathbf{k},-\omega)}\bigg|_{h=\widetilde{h}=0;\mathbf{j},\widetilde{\mathbf{j}}=\mathbf{0}},
$$

$$
\langle\widetilde{\mathbf{v}}(\mathbf{k},\omega)\rangle=\frac{-\delta F[h,\widetilde{h},\mathbf{j},\widetilde{\mathbf{j}}]}{\delta\widetilde{\mathbf{j}}(-\mathbf{k},-\omega)}\bigg|_{h=\widetilde{h}=0;\mathbf{j},\widetilde{\mathbf{j}}=\mathbf{0}}.\quad (10)
$$

The functional Γ generates vertex functions which can be obtained diagrammatically by keeping only one-particle-irreducible (1PI) graphs and amputating the external legs.

The evaluation of the two-point correlation function $\langle N(\mathbf{k},\Omega)N(\mathbf{k}',\Omega')\rangle$, performed in this work up to one-loop order, may be represented diagrammatically as
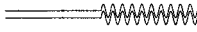

$$\tag{11}$$

where the elements used in constructing Feynman diagrams are easily determined. For example, in expansions about equilibrium, the result is

$$\equiv \frac{1}{-i\omega + D_0 k^2/S^{(eq)}(k)}, \quad (12)$$

$$\equiv \frac{2D_0 n_c k^2}{\omega^2 + \left(\dfrac{D_0 k^2}{S^{(eq)}(k)}\right)^2}, \quad (13)$$

$$\equiv \frac{(\overset{\leftrightarrow}{\Phi}_{\mathbf{k}})^{\alpha\beta}}{-i\omega + \nu k^2}, \quad (14)$$

$$\equiv \frac{2k_B T(\nu/\rho)k^2}{\omega^2 + (\nu k^2)^2}(\overset{\leftrightarrow}{\Phi}_{\mathbf{k}})^{\alpha\beta}, \quad (15)$$

$$\equiv -\frac{i}{2}\,\mathbf{V}_{\mathbf{k}}^{\alpha;\beta\gamma}, \quad (16)$$

$$\equiv \frac{i}{2}\,\mathbf{U}^{\alpha}(\mathbf{k},\mathbf{k}'), \quad (17)$$

$$\equiv -ik^{\alpha}. \quad (18)$$

Note that Eq. (11) can be obtained in alternate ways; we have adopted the MSR method since it can be used as a common starting point for a theory of the dynamic structure factor [which Eq. (11) formally is], for a self-consistent version of the theory, or for an analysis of a linear relaxation experiment. Some of these points are already under consideration, and will be reported later.

This study focuses on such a system being driven away from equilibrium by the application of linear shear, i.e.,

$$\mathbf{v}(\mathbf{x},t) = \mathbf{v}_0(\mathbf{x}) + \delta\mathbf{v}(\mathbf{x},t), \quad \text{with} \quad \mathbf{v}_0(\mathbf{x}) = \omega_0\hat{\mathbf{y}}x. \quad (19)$$

In all that follows, $\omega_0 \geq 0$ is assumed, with no loss of generality. The shear breaks detailed balance and brings the system to a steady state out of equilibrium. Thus the fluctuation-dissipation relation no longer holds and the system will not decay back to its original thermodynamic equilibrium as long as the external force (shear) persists. The applied shear also modifies the bare propagators that appear in Eq. (11), i.e., it modifies Eqs. (12)–(15). They become nondiagonal in the shear gradient direction of Fourier space, and hence become integral operators as opposed to simple factors. For example, the bare number density response function becomes

$$\Big|_{k_y>0} = \frac{\theta(-(k_x + k_x'))}{\omega_0 k_y}$$

$$\times \exp\left(-i\Omega\frac{(k_x + k_x')}{\omega_0 k_y} - \int_{k_x}^{-k_x'}\frac{dr_x}{\omega_0 k_y}(r_x^2 + k_\perp^2)D(\mathbf{k}_\perp, r_x)\right)$$

$$\Big|_{k_y<0} = \frac{\theta(k_x + k_x')}{(-\omega_0 k_y)}$$

$$\times \exp\left(i\Omega\frac{(k_x + k_x')}{(-\omega_0 k_y)} - \int_{-k_x'}^{k_x}\frac{dr_x}{(-\omega_0 k_y)}(r_x^2 + k_\perp^2)D(\mathbf{k}_\perp, r_x)\right) \quad (20)$$

while the correlation function takes the form

$$\Big|_{k_y>0} = 2D_0 n_c \int \frac{dk_x'}{2\pi}\int_{\max(k_x,-k_x')}^{+\infty}\frac{dl_x}{(\omega_0 k_y)^2}(l_x^2 + k_\perp^2)$$

$$\times \exp\left(-i\Omega\frac{(k_x + k_x')}{\omega_0 k_y} - \int_{k_x}^{l_x}\frac{dr_x}{\omega_0 k_y}(r_x^2 + k_\perp^2)D(\mathbf{k}_\perp, r_x) - \int_{-k_x'}^{l_x}dr_x\,\omega_0 k_y(r_x^2 + k_\perp^2)D(\mathbf{k}_\perp, r_x)\right)$$

$$\Big|_{k_y<0} = 2D_0 n_c \int \frac{dk_x'}{2\pi}\int_{-\infty}^{\min(k_x,-k_x')}\frac{dl_x}{(\omega_0 k_y)^2}(l_x^2 + k_\perp^2)$$

$$\times \exp\left(i\Omega\frac{(k_x + k_x')}{(-\omega_0 k_y)} - \int_{l_x}^{k_x}\frac{dr_x}{(-\omega_0 k_y)}(r_x^2 + k_\perp^2)D(\mathbf{k}_\perp, r_x) - \int_{l_x}^{-k_x'}\frac{dr_x}{(-\omega_0 k_y)}(r_x^2 + k_\perp^2)D(\mathbf{k}_\perp, r_x)\right) \quad (21)$$

where $\mathbf{k}_\perp \equiv (0, k_y, k_z)$. This constitutes a nontrivial change which greatly increases the complexity of the calculation. The leading order correlation function, cf. Eq. (21), is equivalent to the result of Ronis [7].

Previous studies of sheared colloid suspensions dealing with the liquid phase either ignored the effect of the solvent [18,11], or dealt with convection only to zero-loop order [7]. As a consequence, these methods were unsuccessful at producing an effect in the gradient direction (here $\hat{\mathbf{x}}$). As can be seen from the modified response and correlation functions, Eqs. (20) and (21), respectively, the shear strength ω_0 couples to the component of the wave number in the flow direction, k_y; hence, in the plane perpendicular to $\hat{\mathbf{y}}$, the hydrodynamic model implies that only mode-coupling terms could lead to shear effects, and these first appear in the one-loop terms of Eq. (11).

As was shown in Ref. [7], the zero-loop expressions, Eqs. (20) and (21), predict a loss of order as the shear is increased, eventually resulting in an ideal gas structure factor, i.e., $S^{(eq)}(\mathbf{k}) \simeq 1$, as long as $k_y \neq 0$. When $k_y = 0$ the leading order analysis predicts no change in the structure factor. The reason for this behavior lies in the form of the response function, cf. Eq. (20); it is unchanged for $k_y = 0$ but when $k_y \neq 0$ it becomes a rapidly decreasing function of $\mathbf{k}, \mathbf{k}'$. At higher order, even though the loop terms in Eq. (11) include contributions from internal wave vectors that are orthogonal

to y, the external propagators (lines) will cause the result to be negligibly small for large shears unless $k_y = 0$, and hence we focus our attention on wave vectors in the gradient direction. Moreover, note that the zero-loop analysis describes the distortion of the structure factor reasonably well away from the gradient axis, i.e., for $k_y \neq 0$.

Thus we focus on evaluating the nonlinear correction along the gradient direction and proceed to evaluate, to first order in perturbation theory, the two-point correlation function for the colloid number density, setting k_y and k_z to zero. This will be done for a general equilibrium structure factor $S^{(eq)}(\mathbf{k})$.

The quantity of interest is the equal-time two-point correlation function. It is related to the dynamical two-point correlation function and to the nonequilibrium structure factor in the following way:

$$\langle N(\mathbf{k})N(\mathbf{k}')\rangle = \int \frac{d\Omega}{2\pi} \int \frac{d\Omega'}{2\pi} \langle N(\mathbf{k},\Omega)N(\mathbf{k}',\Omega')\rangle$$
$$\equiv (2\pi)^d \delta(\mathbf{k}+\mathbf{k}') n_c S(\mathbf{k}). \qquad (22)$$

To one-loop order, cf. Eq. (11), the equal-time structure factor along the special direction $\hat{\mathbf{x}}$ becomes

$$S(t) = S^{(eq)}(t)\{1 + S^{(eq)}(t) n_c [f(t) + f(-t)]\}, \qquad (23)$$

where the nonequilibrium correction $n_c f(t)$ has the form

$$n_c f(t) = \frac{3}{4\pi^2}\left(\frac{a}{\sigma}\right)\int d\mathbf{x}\frac{\mathbf{x}_\perp^2}{[\mathbf{x}_\perp^2 + (x+t)^2]^2}\int_0^{+\infty} dp \frac{\partial}{\partial p}\left(\frac{S^{(eq)}(\sqrt{\mathbf{x}_\perp^2 + (p+x)^2})}{S^{(eq)}(|\mathbf{x}|)}\right)\exp\left[-\frac{1}{\alpha y}\int_0^p dr\frac{[\mathbf{x}_\perp^2 + (r+x)^2]}{S^{(eq)}(\sqrt{\mathbf{x}_\perp^2 + (r+x)^2})}\right], \qquad (24)$$

with $\mathbf{x}_\perp \equiv (0, y, z)$, and with the integration domain along the y direction restricted to $y \geq 0$. The quantity $n_c f(t)$ is a function of the scaled wave number $t \equiv k_x \sigma$ [where $\sigma \simeq 2\pi/k_{max}$ is the characteristic length scale defined by the maximum of $S^{(eq)}(k)$, which for hard spheres corresponds to the particles' diameter], the dimensionless quantity $\alpha \equiv \omega_0 \sigma^2/(2D_0)$, which is analogous to the Péclet number and is sometimes called the Deborah number [29], and the packing fraction, $\eta \equiv (4\pi/3) n_c a^3$, a being the radius of the particles. Note that the latter expression does not have an explicit dependence on the kinematic viscosity ν, but only an implicit one through D_0, if one accepts the Stokes-Einstein relation. Further details on the derivation of $f(t)$ are given in the Appendix.

The equilibrium structure factor is related to the direct correlation function through the Ornstein-Zernike relation,

$$S^{(eq)}(t) = \frac{1}{1 - n_c \widetilde{c}(t)}, \qquad (25)$$

where $\widetilde{c}(t)$ is the Fourier transform of the equilibrium direct correlation function $c(x)$. If the Ornstein-Zernike form is assumed for the nonequilibrium structure factor, cf. Eq. (25), then the first-order correction to a nonequilibrium direct cor-

relation function is easily found from Eqs. (23) and (25) and leads to the following resummed expression for S:

$$1/S(t) = 1 - n_c[\widetilde{c}(t) + f(t) + f(-t)]. \qquad (26)$$

This formulation will be particularly useful later when constructing an approximate stability phase diagram. The instability in question is then simply defined as the $1/S(t^*)|_{\alpha=\alpha_{cr}} = 0$, which corresponds to a spinodal line, where $t^* = k_x^* \sigma$ is the position of the diverging peak in the structure factor.

It is of interest to investigate the nonequilibrium structure factor in the limit of small shear ($\alpha < 1$), as well as its asymptotic infinite-shear behavior ($\alpha \to \infty$), as simplified expressions for the nonlinear correction $f(t)$ may be obtained. For small Deborah numbers and at $t = 0$, the full expression for $f(0)$, cf. Eq. (24), reduces to

$$\lim_{\alpha \to 0} n_c f(0) = \frac{3}{4\pi^2}\left(\frac{a}{\sigma}\right)\alpha^{3/2}\frac{[\partial^2 n_c \widetilde{c}(t)/\partial t^2]|_{t=0}}{[1 - n_c \widetilde{c}(0)]^{5/2}}C, \qquad (27)$$

where C is a constant given by Eq. (A6) in the Appendix. Hence it is natural to suppose that quantities which mainly depend on the long wavelength behavior of the system are expected to vary as $\alpha^{3/2}$ for small α.

At finite t, the nonequilibrium correction to the direct correlation function is

$$n_c f(t) = n_c f(-t) = \frac{3}{64} \left(\frac{2a}{\sigma} \right) \left(\frac{\alpha}{t} \right)^2 \int_0^\infty \frac{dr}{r} \frac{n_c \tilde{c}'(r)}{[1 - n_c \tilde{c}(r)]^3} \left[\frac{(x^2 - 1)}{x} \ln \left| \frac{1+x}{1-x} \right| \left(3x^4 + \frac{5}{4}x^2 + \frac{5}{4} + \frac{7}{4x^2} + \frac{3}{4x^4} \right) \right.$$
$$\left. - 6x^4 + \frac{3}{2}x^2 - \frac{1}{30} + \frac{5}{2x^2} + \frac{3}{2x^4} \right], \tag{28}$$

where $x \equiv r/t$. In addition to the requirement of small-shear-rate ($\alpha < 1$), the validity of the finite-t expression is restricted to the regime where $\alpha^{1/2} < t$, and hence the notion of a boundary layer arises. Equation (28) will be compared with the numerical integration of the full expression for hard spheres, confirming the existence of a boundary layer as defined above.

Nonanalyticities were seen in simulations of fluids with various types of interaction [30–33], where the typical behavior was an increase in pressure as $\omega_0^{3/2}$ for small to intermediate shear rates, and a decrease of the viscosity as $\omega_0^{1/2}$ for intermediate shear rates. Theoretically, nonanalytical behavior was also found [34–36,16,9], together with an expansion parameter analogous to α/t^2 for quantities such as the structure factor which implies the same boundary layer definition as above. Note that the relation between the structure and the viscosity is nontrivial, and has contributions from both high and low wave numbers; hence, just which wave number regime, if any, makes the dominant contribution is responsible for the variety of different behaviors seen in simulations and experiment [16].

Simple expressions are also found for the infinite-shear correction to the direct correlation function:

$$n_c f_\infty(t) + n_c f_\infty(-t) = -\frac{3}{4\pi} \left(\frac{a}{\sigma} \right) \int_0^\infty dx \frac{x^2}{t^2} n_c \tilde{c}(x) \left(\frac{x^2 + t^2}{xt} \ln \left| \frac{x+t}{x-t} \right| - 2 \right), \tag{29}$$

where $x = q\sigma$ is the scaled internal momentum, and t is defined above. The same quantity may be expressed in terms of the real space correlation function $c(s)$, where $s \equiv r/\sigma$ is a scaled real space variable, giving

$$n_c f_\infty(t) + n_c f_\infty(-t) = -6\pi \left(\frac{a}{\sigma} \right) \sigma^3 \int_0^\infty ds \frac{n_c c(s)}{st^2} \left(\frac{\sin(st)}{st} [(st)^2 - 1] + \cos(st) \right). \tag{30}$$

The notion of infinite-α limit may appear purely academic, since experimentally, the maximum shear rates attainable is of the order of 10^3–10^4 s^{-1}, which for neutral particles of radius $a = 10^{-5}$ cm in water at room temperature gives $\alpha_{max} \simeq 10$–100 as the largest Deborah number which can be achieved. However, substituting glycerine for water and increasing the size of the particles twofold boosts the Deborah number dramatically, to $\alpha_{max} \simeq 10^4$–10^5, which may now be considered the $\alpha \gg 1$ regime, if not the infinite-α limit. Hence, in practice, the limit of infinite shear may be approached by increasing the Deborah number $\alpha \gg 1$, while keeping the Prandtl number at a very small value, $P_t \ll 1$, and ω_0 small enough to avoid any effect on the solvent such as turbulence, i.e., $\omega_0 l^2 / \nu \ll R_{cr}$, where l is the plate separation in the shear gradient direction and R_{cr} is the critical Reynolds number.

III. RESULTS

The correction to the nonequilibrium structure factor, $f(t)$, presented in the preceding section has been evaluated numerically for a system of hard spheres at both low and high packing fraction. Again the reader is reminded that the results reported below relate to the distortion of the equilibrium structure factor caused by the application of a shear stress, and our attention is focused on the gradient shear direction as we believe this is where the most interesting effects arise.

The well-known Percus-Yevick expression for the real space correlation function is

$$c_{PY}(x) \equiv \begin{cases} -\lambda_1 + 6\eta \lambda_2 x - \frac{1}{2}\eta \lambda_1 x^3, & x \leq 1 \\ 0, & x > 1 \end{cases} \tag{31}$$

where

$$\eta \equiv \frac{4\pi}{3} a^3 n_c, \quad \lambda_1 \equiv \frac{(1+2\eta)^2}{(1-\eta)^4}, \quad \lambda_2 \equiv \frac{(1+\eta/2)^2}{(1-\eta)^4}, \tag{32}$$

with $x \equiv r/\sigma$, where r is the length of the Cartesian vector $\mathbf{r}$ and, as mentioned earlier, σ is the scale of the structure factor, which for hard spheres corresponds to the diameter of the particles, that is $\sigma = 2a$, and henceforth, when dealing with hard-sphere systems, the ratio $\sigma/(2a)$ appearing in Eq. (23) will be set to one. Besides being widely used to fit experimental data, this type of model, because of its simplicity, allows the analysis to be carried out farther in some cases, thus reducing the need for numerical computation. For example, in the limit of small shear, $\alpha < 1$, and at zero wave number, a closed expression emerges for the correction to the structure factor, $f(0)$, which shows a simple dependence on the shear rate. Namely, for hard spheres, Eq. (27) reduces to

$$\lim_{\alpha \to 0} n_c f(0) = \frac{3C}{\pi^2} \alpha^{3/2} \frac{\eta(\lambda_1/5 - \eta\lambda_2 + \eta\lambda_1/16)}{[1 + \eta(8\lambda_1 - 36\eta\lambda_2 + 2\eta\lambda_1)]^{5/2}}, \tag{33}$$

where C is given by Eq. (A6). Comparison of the small-shear approximation Eq. (33) with the full expression Eq. (24) is shown in Fig. 1 where $f(0)$ is plotted versus $\alpha^{3/2}$ at infinite dilution; excellent agreement is seen for $\alpha \lesssim 1$.

At nonzero values of wave vector ($t \neq 0$), the small-shear expression Eq. (28) is shown in Table I to be reasonably accurate for $\alpha^{1/2} \lesssim t$. Consequently, at least for hard-sphere systems in the limit of small-shear rates, there seems to be a

boundary layer around $t \simeq \alpha^{1/2}$, outside which the correction to the direct correlation function, $n_c[f(t) + f(-t)]$, has an α^2 dependence. Note that there are similar boundary layers in the asymptotic expansions of the zero-loop results for $k_y \neq 0$ [7,16,9].

A simple expression is also obtained in the limit of an infinite-shear rate. Substituting $c_{PY}(s)$ given by Eq. (31), in Eq. (30) for the asymptotic infinite-shear nonequilibrium correction, yields the following closed expression:

$$
n_c f_\infty^{PY}(t) + n_c f_\infty^{PY}(-t) = 18\eta\lambda_1 \frac{1}{t^2}\left[\frac{\sin(t)}{t} - \cos(t)\right] + 108\eta^2\lambda_2 \frac{1}{t^2}\left[\frac{1}{t}\left(\frac{\pi}{2} + \mathrm{si}(t)\right) + \cos(t) - 2\frac{\sin(t)}{t}\right]
$$

$$
+ 9\eta^2\lambda_1 \frac{1}{t^4}\left[4t\sin(t) - t^2\cos(t) + 9\left(\cos(t) - \frac{\sin(t)}{t}\right)\right], \tag{34}
$$

where

$$
\mathrm{si}(t) \equiv -\int_t^\infty [\sin(x)/x]dx, \tag{35}
$$

and η, λ_1, and λ_2 are defined in Eq. (32).

We first examine a system of hard spheres at infinite dilution, and consider $\lim_{\eta \to 0}[S(t) - 1]/\eta$, which, from Eq. (26), is just $(6/\pi\sigma^3)[\tilde{c}(t) + f(t) + f(-t)]$. The latter quantity is shown in Fig. 2 for different orders of magnitude in shear together with the corresponding equilibrium quantity, i.e., the direct correlation function at zero packing fraction. The main trends to note are the flattening of the nonequilibrium correlation function and the slight shift of the main peak to larger wave numbers at small-shear rate, and then to smaller wave numbers at higher-shear rate. The inset depicts the quantity $(6/\pi\sigma^3)[f(t) + f(-t)]$ for the same shear rates
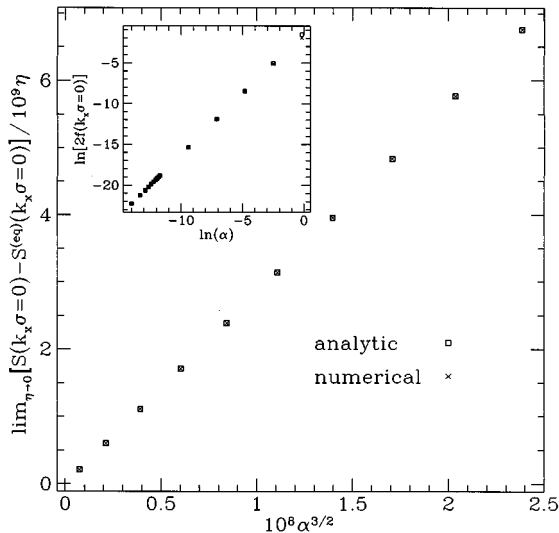
as the main figure, as well as the direct correlation function. It is clearly seen that short-range order in the gradient direction monotonically decreases as shear increases, at infinite dilution. This is contrary to the theoretical results of Blawzdziewicz and Szamel, cf. Fig. 2 of Ref. [11], who predict that shear will enhance short-range order at infinite dilution, the exact opposite of our conclusion.

Of course, our theory is not restricted to infinite dilution and Figs. 3 and 4 show the nonequilibrium structure factor at various shear rates and at a packing fraction of 10% and 50%, respectively. The insets depict the corresponding quantity $[S(t) - S^{(eq)}(t)]/S^{(eq)}(t)$, the deviation from equilibrium, for the different shear rates. Again, note the flattening of the structure factor with increasing shear, as well as the peak position which initially moves right and then left, as the shear rate is further increased; both these effects have been observed in the experiment of Ackerson et al. when looking at the structure factor in the gradient direction [17]. Hence, at low packing fraction, the effect of increasing shear is to decrease the correlations between the colloidal particles (a behavior also seen in the flow direction, i.e., for $k_y \neq 0$ [7]), e.g., as if the packing fraction were reduced.

The monotonic rise of the structure factor at long wavelengths ($t \ll 1$) as a function of the Deborah number α persists as the concentration increases. For the case at hand, i.e., the Percus-Yevick approximation for a hard-sphere system, at some point it will even cross one $[S(0)|_{\alpha=\infty} = 1]$ at a packing fraction of 55.8%, and will eventually become un-

FIG. 1. Comparison of the small-shear approximation expression at $k_x\sigma = 0$, which has an $\alpha^{3/2}$ behavior, cf. Eq. (27), and the exact numerical result, for a system at infinite dilution. The same quantity is shown on a log-log scale in the inset. Good agreement is seen for $\alpha < 1$.

TABLE I. Comparison between direct numerical integration of Eq. (24) with the small-shear finite-t expression Eq. (28). Good agreement is seen for $t \gtrsim \alpha^{1/2}$.

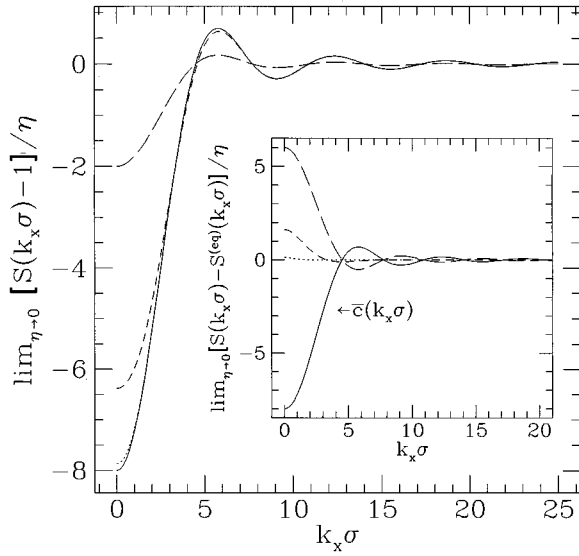| η	α	t	Exact result	Approximation	%Δ
0.1	1.0	6.0	-9.40277×10^{-5}	-9.42971×10^{-5}	0.3
0.1	1.0	1.0	1.81198×10^{-3}	1.72573×10^{-3}	-4.8
0.1	1.0	0.1	4.68655×10^{-3}	1.62430×10^{-2}	246
0.1	0.1	6.0	-9.30518×10^{-7}	-9.42971×10^{-7}	1.3
0.1	0.1	0.316	5.64058×10^{-5}	5.34716×10^{-5}	-5.2
0.1	0.1	0.03	1.43858×10^{-4}	5.32846×10^{-4}	270

FIG. 2. The zero density limit of the correlation function for hard spheres. The various curves correspond to equilibrium (zero shear, solid line), $\alpha = 0.91$ (short-dashed line), $\alpha = 9.1$ (dashed line), and infinite shear (long-dashed line). Flattening of the curve with increasing shear is clearly seen, as is a slight shift of the main peak to the right at small shear and a shift to the left at infinite shear. The inset depicts the direct correlation function and the nonequilibrium corrections separately.
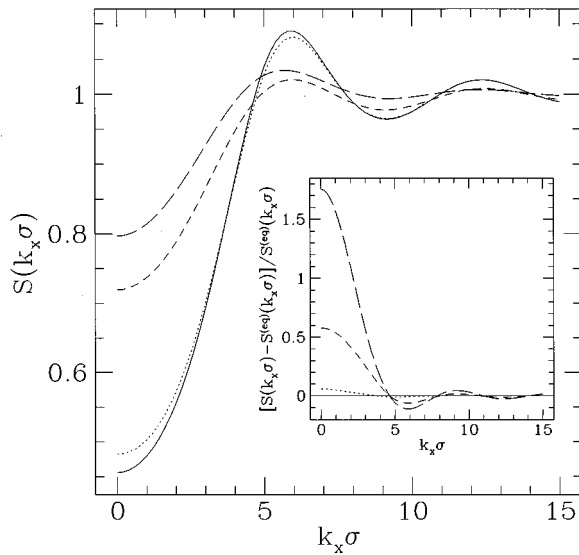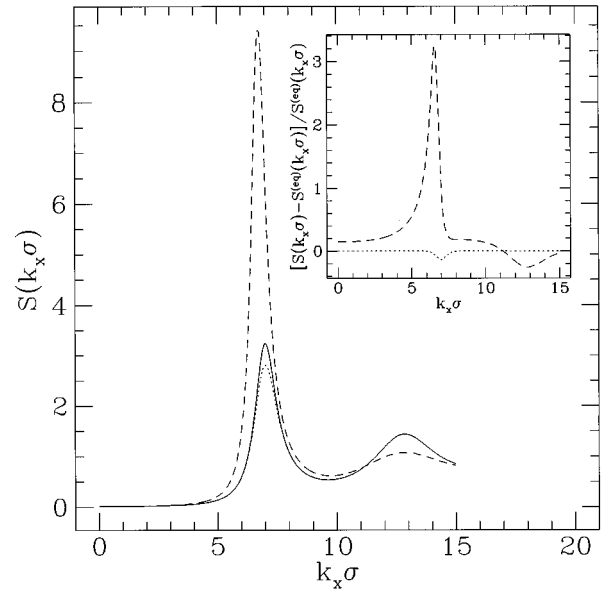

FIG. 4. The same quantities as in Fig. 3, but for a packing fraction of 50%, and again for $\alpha = 0$ (solid line), $\alpha = 10$ (short-dashed line), and $\alpha = 500$ (dashed line). At infinite shear, the system is unstable, and hence the omission of the $\alpha = \infty$ curve. As in the previous two figures, the main peak first moves right and then left, and at small wave numbers, the structure factor moves up continuously. The main peak first decreases, but then moves up dramatically, signaling that the system is close to the spinodal point, presumably representing an instability to the formation of lamella in the shear gradient direction. The inset shows the nonequilibrium correction to the direct correlation function multiplied by the nonequilibrium structure factor for the parameters mentioned above.

FIG. 3. Nonequilibrium structure factor, also in the shear gradient direction but for a packing fraction of 10%, for $\alpha = 0$ (solid line), $\alpha = 10$ (short-dashed line), $\alpha = 500$ (dashed line), and infinite shear (long-dashed line). As before, the main peak initially moves to higher wave numbers, then turns back and moves to lower values of $k_x \sigma$ at larger shear rates, while at long wavelengths, the structure factor increases monotonically. The main peak, however, at first decreases with increasing shear but later starts increasing again for large values of α, while the secondary peaks continue to flatten. The quantity shown in the inset represents the nonequilibrium corrections times the nonequilibrium structure factors $[f(k_x \sigma) + f(-k_x \sigma)]S(k_x \sigma)$, for the shear rates cited above.

stable $[1/S(0)|_{\alpha = \infty} = 0]$ when η reaches 57.3%. Hence, at very large values of the shear rate and of the concentration, large, long-wavelength fluctuations develop, a situation which is reminiscent of systems near a second-order phase transition. However, as we now show, an instability near the principal peak of the structure factor occurs at smaller packing fraction (or equivalently, for weaker interactions), which renders the long-wavelength instability irrelevant.

At larger packing fractions, the amplitude of the main peak of the structure factor will first decrease as α is increased, reach a minimum, and thereafter increase. We illustrate this in Fig. 5, which shows the difference $[S(t^*)|_{\alpha = \infty} - S^{(eq)}(t^*)]$ between the nonequilibrium structure factor at infinite shear and the equilibrium structure factor as a function of the packing fraction η (each structure factor being evaluated at its maximum peak position t^*). At small concentrations, the latter quantity is negative, which implies the peak has decreased as the shear rate was increased from zero to infinity, while at larger concentrations it becomes positive, implying the existence of more short-range order at infinite shear than at equilibrium.

Hence, while for large length scales, fluctuations increase monotonically, the situation is different in the first peak region. Initially, when the concentration is very small, the effect of shear is the same as for large wavelengths, i.e., less order. However, as the number of particles per unit volume increases, a weak order develops in the gradient direction as to avoid the active-mixing hydrodynamic interactions cre-
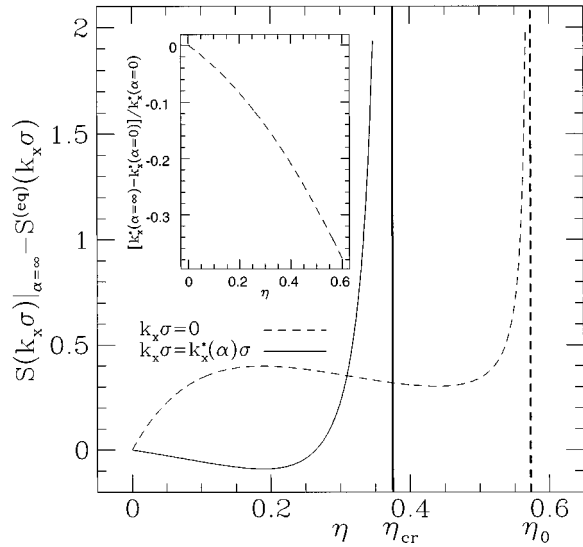
FIG. 5. Shown here is the difference in height between the non-equilibrium structure factor at infinite shear and the equilibrium structure factor, both at long wavelengths (dashed line) and for the main peak (solid line). The main peak is lower at $\alpha = \infty$ for packing fractions less than 26–27%, while for small wave numbers, it is always higher. The inset depicts the motion of the main peak at infinite shear, relative to its position at equilibrium, as a function of packing fraction. As shown, the peak always moves to the left for asymptotically high shear rates, and at large enough packing fractions, by a sizable amount, up to 20–30%.
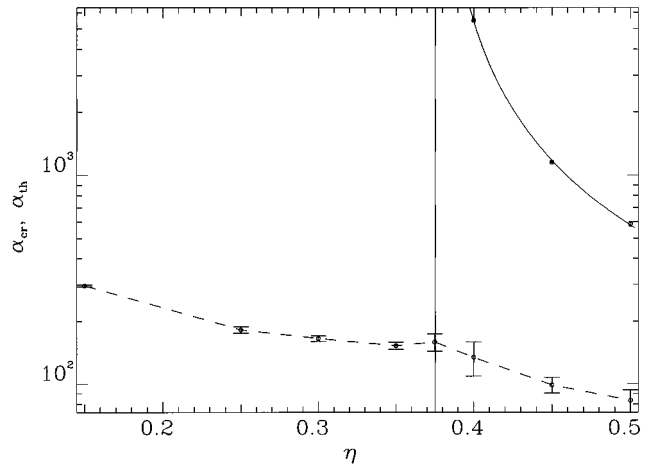

FIG. 6. Phase diagram showing the spinodal line (solid line) representing an instability to the formation of lamella in the shear gradient direction. Above this line, the system is unstable to the formation of lamellae perpendicular to the velocity. The solid line shows $|\eta - \eta_{cr}|^{-z}$, where $z = 1.4$ (as determined by least squares fitting to the data points). Also shown is the line where $[\partial S(t^*)/\partial \alpha] = 0$ (t^* being the main peak position), which may roughly correspond to the transition between the shear thinning behavior and shear thickening for reasons explained in the text. The points on these lines were obtained in the following manner: First, a set of points were calculated numerically in the α-t plane for a given value of η. The resulting two dimensional grid was fitted to various polynomials in α and t and the transition points were determined numerically. The data points represent the average of the results, with one standard deviation error bars.

ated by the increasingly sheared solvent. Eventually, a critical value is reached, $1/S(t^*)|_{\eta_{cr};\alpha = \infty} = 0$, characterized by a diverging peak in the structure factor. Note that the latter instability corresponds to a spinodal point, thus implying the possibility of a fluctuation induced first-order transition before the point in question is reached. Moreover, in the Percus-Yevick model, there is a critical packing fraction, easily found numerically using Eq. (34), below which no instability occurs (even at infinite shear). Its value is $\eta_{cr} = 0.375\,319\,51$.

Since the viscosity of the whole system is proportional to the integral of $[S(k) - 1]$ times other factors [16], the shear-thinning and -thickening behaviors as well as discontinuous jumps in viscosity are probably related to the initial flattening of the structure factor followed by the increase in the peak up to the instability. Indeed, this suggests that the region of parameters where the first peak of the structure factor goes from a decreasing to an increasing behavior, which may be defined as $\partial S(t^*)/(\partial \alpha) = 0$ with t^* the position of the first peak, might correspond to the point where the system reverses its shear-thinning behavior and starts shear thickening. For packing fractions higher than the critical value, the correlations decrease [i.e., $S(k) \rightarrow 1$ for all k's except for those near the first peak in $S^{(eq)}(k)$]. The correlations in this range at some point start to increase, until eventually they diverge at a large but finite value of α, the Deborah number.

A phase diagram may be drawn for $\eta > \eta_{cr}$, in the η-α plane, together with a line delimiting the shear-thinning behavior from shear thickening. Such a diagram is shown in Fig. 6. Below the spinodal line (full line), the system may be characterized as liquidlike, whereas above the transition line

the system is unstable against the formation of layers perpendicular to the shear gradient direction. Since near the instability the structure factor develops a large peak, drastic changes in quantities associated with it are expected, in particular in the average stress tensor $\langle \tau^{ij} \rangle$ and thereby the viscosity. The dotted line in the same figure shows where the liquidlike system is expected to stop shear-thinning and start shear thickening, as characterized by the behavior of the first peak of the structure factor.

IV. CONCLUSION

The effect of linear shear on a system of colloidal suspensions was studied using a stochastic field model describing the evolution of the local particle number density $N(\mathbf{x}, t)$ and the local solvent velocity $\mathbf{v}(\mathbf{x}, t) = \omega_0 x \hat{\mathbf{y}} + \delta \mathbf{v}(\mathbf{x}, t)$. The main conclusions are as follows.

At small shear rates ($\alpha < 1$), the nonequilibrium correction to the correlation function at zero wave number increases as $\alpha^{3/2}$, implying $S(0)$ grows accordingly, and hence, such a behavior should be observed in any experimental quantity or numerical simulation probing the long-wavelength character of the system. For finite values of wave number, the concept of boundary layer emerges, defined by $k_x \sigma \simeq \alpha^{1/2}$. When $k_x \sigma \gtrsim \alpha^{1/2}$, again for small-shear rates, the nonequilibrium correction is well approximated by Eq. (28), which shows an α^2 dependence.

As the shear is gradually increased to infinity, the structure factor is modified in different ways depending on the

strength of interaction between the colloidal particles and on the magnitude of the wave vector. The structure factor approaches unity for all wave vectors except those in the neighborhood of the first peak with $k_y \neq 0$; here, the main peak first decreases with increasing shear, but, if the interparticle interactions are strong enough (e.g., by having the concentration high enough), it eventually reaches a minimum and then grows. This represents increasing short-range order, and eventually, an instability may be reached, characterized by a diverging peak. This divergence in the main peak of the structure factor usually indicates that some type of long-range order has settled in. A phase diagram was thus obtained in the Percus-Yevick approximation. The line in the α-η plane divides a liquidlike region from a region where lammella are thought to form in the plane perpendicular to the x direction (the shear gradient direction). A lower limit to the packing fraction is thus found for a hard-sphere system, below which no instability occurs even at infinite shear; i.e., no instabilities are possible for packing fractions less than 37.5%, in hard-sphere systems. Note that these last two observations do not preclude the existence of first-order transitions that may occur on either side of the $\eta = \eta_{cr}$ line.

The aforementioned changes in the structure factor as a function of Deborah number and packing fraction and its relation to the viscosity (as proportional to the integral of $[S(k)-1]$), leads to a line delimiting shear-thinning and shear-thickening behavior [here defined as $\partial S(t^*)/(\partial \alpha) = 0$ for simplicity], and is indicated in the phase diagram.

At low particle concentrations, it is interesting to note that the reduction in the amplitude of the main peak together with a shift of the latter to lower wave numbers was seen experimentally by Ackerson et al. [17] when looking at the structure factor in the gradient direction.

Finally, in charged systems, an instability may occur at much smaller packing fraction than the lower critical packing fraction of 37.5% found for hard-sphere systems for the obvious reason that charged particles in poorly screened suspensions have strong electrostatic interactions, and hence have an effective size which is significantly larger than their physical size.

Hence the model of colloidal suspension presented in this paper has succeeded in reproducing many results previously seen in experiments or numerical simulations. In addition, predictions were made in the form of a phase diagram, among other things, which, at least in the case of hard spheres, may easily be compared with experiments and numerical simulations using the simple parameters α and η, the Deborah number and the packing fraction, respectively.

We have compared the predictions of the theory with the trends observed by Ackerson et al. [17]; the correspondence with simulations is more difficult to establish since to date none of them include a real solvent, thereby making the identification of the Deborah number problematic. Nonetheless, what we predict is consistent with what is seen experimentally. This may be somewhat fortuitous since the de Gennes form for the diffusion constant will cease to be valid for very concentrated suspensions and higher-order corrections in perturbation theory will likely be important near the spinodal lines.

APPENDIX

The expression corresponding to the nonequilibrium structure factor up to one-loop corrections, cf. Eq. (11), for external wave numbers in the gradient direction is

$$S(k_x) = S^{(eq)}(k_x)\{1 + S^{(eq)}(k_x)[F(k_x) + F(-k_x)]\},$$
(A1)

where

$$
\begin{aligned}
F(k_x) = &\frac{k_B T}{\rho} D_0 n_c \int \frac{d\mathbf{q}}{(2\pi)^d} \frac{q_\perp^2}{q^2} \int_{q_x}^{+\infty} \frac{dl_x}{\omega_0 q_y} \exp\left[\left(\frac{D_0 k_x^2}{S^{(eq)}(k_x)} + \nu[\mathbf{q}_\perp^2 + 1/3(q_x^2 + q_x l_x + l_x^2)]\right) \frac{(q_x - l_x)}{\omega_0 q_y}\right. \\
&+ \int_{k_x - q_x}^{k_x - l_x} \frac{dr_x}{\omega_0 q_y} \frac{D_0(\mathbf{q}_\perp^2 + r_x^2)}{S^{(eq)}(\sqrt{\mathbf{q}_\perp^2 + r_x^2})}\right]\left\{\left(\frac{S^{(eq)}(\sqrt{\mathbf{q}_\perp^2 + (k_x - l_x)^2})}{S^{(eq)}(k_x)} - 1\right) \frac{2}{\mathbf{q}_\perp^2 + l_x^2} \int_{l_x}^{+\infty} dp_x p_x \exp\left(2\nu[\mathbf{q}_\perp^2 + 1/3(l_x^2 + l_x p_x\right.\right. \\
&\left.+ p_x^2)]\frac{(l_x - p_x)}{\omega_0 q_y}\right) + \int_{l_x}^{+\infty} dp_x \left(\frac{\partial}{\partial p_x} \frac{S^{(eq)}(\sqrt{\mathbf{q}_\perp^2 + (k_x - p_x)^2})}{S^{(eq)}(k_x)}\right) \exp\left(2\int_{k_x - l_x}^{k_x - p_x} \frac{dr_x}{\omega_0 q_y} \frac{D_0(\mathbf{q}_\perp^2 + r_x^2)}{S^{(eq)}(\sqrt{\mathbf{q}_\perp^2 + r_x^2})}\right) \\
&\left.\times\left[\frac{S^{(eq)}(k_x)}{S^{(eq)}(\sqrt{\mathbf{q}_\perp^2 + (k_x - l_x)^2})} + \frac{2}{\mathbf{q}_\perp^2 + l_x^2} \int_{l_x}^{+\infty} dp_x' p_x' \exp\left(2\nu[\mathbf{q}_\perp^2 + 1/3(l_x^2 + l_x p_x' + p_x'^2)]\frac{(l_x - p_x')}{\omega_0 q_y}\right)\right]\right\},
\end{aligned}
$$
(A2)

where $\mathbf{q}_\perp \equiv (0, q_y, q_z)$, and the domain of integration of q_y is restricted to $q_y \geq 0$. Note that the above expression is not symmetric with respect to the k_x origin, so one must add the $-k_x$ contribution to the final result, as shown in Eq. (23). In the above expressions, ν is the kinematic viscosity of the solvent, D_0 corresponds to the diffusion constant of the suspensions and is defined by the Stokes-Einstein relation

$D_0 = k_B T/(6\pi a \nu \rho)$, ω_0 is the shear strength, k_x is the wave number in the direction of the shear gradient, and σ is the scale of the structure factor and is typically defined such that the main peak of the structure factor occurs near $k\sigma \simeq 2\pi$. In the case of hard spheres, for example, σ is the diameter of the colloid particles.

It is thus natural to define new variables as $\mathbf{x} = \mathbf{k}\sigma$,

$p = p_x \sigma$, $p' = p'_x \sigma$, $l = l_x \sigma$, $r = r_x \sigma$, and $t = k_x \sigma$, from which two decay scales appear inside the exponentials, namely, $\beta = \omega_0 \sigma^2/(2\nu)$ (which is similar to the internal Reynolds number $\omega_0 a^2/\nu$) for the solvent velocity propagator, and $\alpha = \omega_0 \sigma^2/(2D_0)$ for the colloid number density propagator. Typically, colloidal suspensions are characterized by small Prandtl number, $P_t = D_0/\nu \ll 1$, implying $\beta \ll \alpha$ and accordingly $\exp[-g_v(l,p,q)/\beta] \ll \exp[-g_N(l,p,q)/\alpha]$ (these exponential factors appear in the expression for F above and are essentially the number density and velocity propagators of the sheared system), where g_v and g_N are functions of the same order of magnitude. This implies that the shear rates relevant to the suspension are orders of magnitude smaller than those relevant to the solvent. Thus the effect of shear on velocity fluctuations is negligible and the usual linear propagator may be used in place of the more tedious expression used at finite shear. This corresponds to neglecting the exponential factors of lines 2 and 4 of Eq. (A2), and integrating by parts over l_x the exponential factor of line 1 and neglecting the remaining integral.

The simplified expression resulting from neglecting terms of order $P_t^{1/2}$ and higher (as described above) is

$$F(t) \simeq f(t) + O(P_t^{1/2}) + \ldots , \qquad (A3)$$

where $f(t)$ is given by Eq. (24).

Even though neglecting terms of $O(P_t^{1/2})$ allows for considerable simplification, the expression remains intractable analytically. Further progress may be achieved by performing an integration by parts in p, and $f(t)$ becomes

$$f(t) = f_\infty(t) + \Delta f(t), \qquad (A4)$$

where f_∞ is the infinite-shear correction given by either of Eqs. (29) or (30), and Δf contains the remaining finite-α dependence. Through a change of variables, specifically, setting $z = \sqrt{x_\perp^2 - y^2}$, the y integration may be carried out, giving

$$\Delta f(t) = \frac{3}{2\pi^2 \alpha}\left(\frac{a}{\sigma}\right) \int_{-\infty}^{+\infty} dx \int_0^\infty dx_\perp \frac{\mathbf{x}_\perp^2}{[\mathbf{x}_\perp^2 + (x+t)^2]^2 S^{(eq)}(|\mathbf{x}|)}$$

$$\times \int_0^\infty dp [\mathbf{x}_\perp^2 + (p+x)^2] \hat{c}[\sqrt{\mathbf{x}_\perp^2 + (p+x)^2}] K_0\left(\frac{1}{\alpha x_\perp}\int_0^p dr \frac{[x_\perp^2 + (r+x)^2]}{S^{(eq)}[\sqrt{x_\perp^2 + (r+x)^2}]}\right), \qquad (A5)$$

where $K_0(x)$ is the modified Bessel function. Nonetheless, Δf still has a complicated form, and its evaluation for arbitrary parameters and structure factors must still be done numerically.

The small-shear expression, Eq. (27), is obtained from Eq. (24) at $t=0$ by scaling all the integration variables by $\alpha^{1/2}$ and Taylor expanding quantities dependent on α around $\alpha = 0$. Equation (27) is thus obtained with the constant C given by

$$C = \int_{-\infty}^{+\infty} dx \int_0^\infty dy \int_{-\infty}^{+\infty} dz \frac{\mathbf{x}_\perp^2}{(\mathbf{x}^2)^2} \int_0^\infty dp (p+x) \exp\left[-\frac{p}{y}\left(\mathbf{x}^2 + xp + \frac{p^2}{3}\right)\right], \qquad (A6)$$

with $\mathbf{x}_\perp^2 = y^2 + z^2$, and $\mathbf{x}^2 = x^2 + \mathbf{x}_\perp^2$. The result is $C = 1.848\,739\,49$.

Using the Percus-Yevick approximation for a hard-sphere system, an approximate analytical asymptotic form for $\Delta f(t=0)$ may be found in the limit of large shear. By adding $f_\infty(t=0)$, which is easily obtained from Eq. (34), to $\Delta f(t=0)$, it follows that the nonequilibrium correction to the direct equilibrium correlation function is

$$2 n_c f(0) \simeq 6\eta\left(\lambda_1 - 4\eta\lambda_2 + \frac{1}{5}\eta\lambda_2\right) - \frac{9\eta\lambda_1}{4\alpha}\left(\frac{7\pi^2}{6} + 2\gamma^2 - 8\gamma + 4\gamma\ln(12\alpha) - 8\ln(12\alpha) + 2[\ln(12\alpha)]^2\right) + O\left(\frac{1}{\alpha}\right), \qquad (A7)$$

where γ is Euler's constant. Note that the logarithmic terms result from the slow oscillatory decay of the equilibrium structure factor in the Percus-Yevick approximation, which aside from the value of the coefficient of λ_1 is the same found in a dilute hard-sphere gas; they would disappear for models that have more rapidly decaying structure factors.

[1] P.M. Chaikin, J.M. di Meglio, W.D. Dozier, H.M. Lindsay, and D.A. Weitz, in *Physics of Complex and Supermolecular Fluids*, edited by S. A. Safran and N.A. Clark (John Wiley & Sons, New York, 1987), pp. 65–81.

[2] N.A. Clark, A.J. Hurd, and B.J. Ackerson, Nature (London) **281**, 58 (1979); Phys. Rev. Lett. **50**, 1459 (1983).

[3] D.W. Schaefer and B.J. Ackerson, Phys. Rev. Lett. **35**, 1448 (1975).

[4] J.C. Brown, P.N. Pusey, J.W. Goodwin, and R.H. Ottewill, J. Phys. A **8**, 664 (1975); P.N. Pusey, *ibid.* **8**, 1433 (1975); S. Harris, *ibid.* **8**, L137 (1975).

[5] P.N. Pusey and W. van Megen, in *Physics of Complex and Supermolecular Fluids*, edited by S.A. Safran and N.A. Clark (John Wiley & Sons, New York, 1987), pp. 673–698.

[6] N.A. Clark and B.J. Ackerson, Phys. Rev. Lett. **44**, 1005 (1980).

[7] D. Ronis, Phys. Rev. A **29**, 1453 (1984).

[8] J.F. Schwarzl and S. Hess, Phys. Rev. A **33**, 4277 (1986).

[9] J.K.G. Dhont, J. Fluid Mech. **204**, 421 (1989).

[10] Y. Yan and J.K.G. Dhont, Physica A **198**, 46 (1993).

[11] J. Blawzdziewicz and G. Szamel, Phys. Rev. E **48**, 4632 (1993).

[12] M.J. Stevens, M.O. Robbins, and J.F. Belak, Phys. Rev. Lett. **66**, 3004 (1991).

[13] D.A. Weitz, W.D. Dozier, and P.M. Chaikin, J. Phys. (Paris) Colloq. **46**, C3-257 (1985).

[14] J.-Y. Yuan and D. Ronis, Phys. Rev. E **48**, 2880 (1993).

[15] B.J. Ackerson, in *Physics of Complex and Supermolecular Fluids*, edited by S.A. Safran and N.A. Clark (John Wiley & Sons, New York, 1987), pp. 673–698.

[16] D. Ronis, Phys. Rev. A **34**, 1472 (1986).

[17] B.J. Ackerson, J.B. Hayter, N.A. Clark, and L. Cotter, J. Chem. Phys. **84**, 2344 (1986).

[18] W. Xue and G.S. Grest, Phys. Rev. Lett. **64**, 419 (1990).

[19] P.C. Martin, E.D. Siggia, and H.A. Rose, Phys. Rev. A **8**, 423 (1973).

[20] J.D. Gunton, M. San Miguel, and P. Sahni, in *Phase Transitions and Critical Phenomena*, edited by C. Domb and J.L. Lebowitz (Academic Press, London, 1983), Vol. 8, p. 267.

[21] P.-G. de Gennes, Physica (Utrecht) **25**, 825 (1959).

[22] J. Machta, I. Procaccia, and I. Oppenheim, Phys. Rev. Lett. **42**, 1368 (1979); Phys. Rev. A **22**, 2809 (1980).

[23] K. Kawasaki, Ann. Phys. (N.Y.) **61**, 1 (1970).

[24] B.I. Halperin, P.C. Hohenberg, and E.D. Siggia, Phys. Rev. Lett. **32**, 1289 (1974).

[25] E.D. Siggia, B.I. Halperin, and P.C. Hohenberg, Phys. Rev. B **13**, 2110 (1976).

[26] P.C. Hohenberg and B.I. Halperin, Rev. Mod. Phys. **49**, 435 (1977).

[27] U. Deker and F. Haake, Phys. Rev. A **11**, 2043 (1975).

[28] H.K. Janssen, in *Dynamical Critical Phenomena and Related Topics*, edited by C. P. Enz, Lecture Notes in Physics, Vol. 104 (Springer, Berlin, 1979).

[29] D. Barber and R. Loudon, *An Introduction to the Properties of Condensed Matter* (Cambridge University Press, Cambridge, England, 1989).

[30] D.J. Evans and H.J.M. Hanley, Physica A **103**, 343 (1980); D.J. Evans, Phys. Rev. A **23**, 1988 (1981).

[31] S. Hess and H.J.M. Hanley, Int. J. Thermophys. **4**, 97 (1983).

[32] L.M. Hood, D.J. Evans, and H.J.M. Hanley, J. Stat. Phys. **57**, 729 (1989).

[33] D.J. Evans, S.T. Cui, H.J.M. Hanley, and G.C. Straty, Phys. Rev. A **46**, 6731 (1992).

[34] M.H. Ernst, B. Cichocki, J.R. Dorfman, B. Charma, and H. van Beijeren, J. Stat. Phys. **18**, 237 (1978).

[35] J.C. Rainwater and S. Hess, Physica (Utrecht) **118A**, 371 (1983).

[36] S. Hess and J.C. Rainwater, J. Chem. Phys. **80**, 1295 (1984).